ACCSCIENCE PUBLISHING

International Journal of Bioprinting

ACCEPTED PAPER · MAIN TEXT

DLP-printed macroencapsulated human liver organoids preserve hepatic stellate cell quiescence for transplantation in immunocompetent mice

Paper version: Accepted Paper

Accepted Papers are manuscripts accepted for publication, encompassing all changes made following the peer review process, along with a standard cover page indicating the paper version and an "Accepted Paper" watermark, but excluding any other editing, typesetting or other changes made by AccScience Publishing and/or authors post-acceptance.

Article ID: IJB026140130

Citation: Zhou Z, Li R, Ding X, Li Y, Luo Y, Liang S. DLP-printed macroencapsulated human liver organoids preserve hepatic stellate cell quiescence for transplantation in immunocompetent mice. *Int J Bioprint*. 2026. doi: 10.36922/IJB026140130

Copyright: © 2026 Author(s). This is an Open Access article distributed under the terms of the Creative Commons Attribution License, permitting distribution, and reproduction in any medium, provided the original work is properly cited.

Publisher's Note: AccScience Publishing remains neutral with regard to jurisdictional claims in published maps and institutional affiliations.

AccScience Publishing
RESEARCH ARTICLE
Volume X Issue X (2026)
doi: 10.36922/IJB026140130

DLP-printed macroencapsulated human liver organoids preserve hepatic stellate cell quiescence for transplantation in immunocompetent mice

Running title: DLP-printed organoids maintain HSC quiescence

Zhi Zhou[1†], Ruitong Li[1†], Xiaodong Ding[1], Yixuan Li[1], Yixue Luo[2]*, and Shaojun Liang[1]*

[1] Tianjin Key Laboratory of Life and Health Detection, Life and Health Intelligent Research Institute, School of Materials Science & Engineering, Tianjin University of Technology, Tianjin 300384, China

[2] Biomanufacturing and Rapid Forming Technology Key Laboratory of Beijing, Department of Mechanical Engineering, Tsinghua University, Beijing, 100084, China

† *These authors contributed equally to this work.*

***Corresponding authors:**

Shaojun Liang (liangshaojun@email.tjut.edu.cn)

Yixue Luo (18810763258@163.com)

Citation: Zhou Z, Li R, Ding X, Li Y, Luo Y, Liang S. DLP-printed macroencapsulated human liver organoids preserve hepatic stellate cell quiescence for transplantation in immunocompetent mice. *Int J Bioprint.* 2026. doi: 10.36922/IJB026140130

Received: April 5, 2026
Revised: May 14, 2026
Accepted: May 22, 2026
Published online: May 22, 2026

Copyright: © 2026 Author(s). This is an Open-Access article distributed under the terms of the Creative Commons Attribution License, permitting distribution, and reproduction in any medium, provided the original work is properly cited.

Publisher's Note: AccScience Publishing remains neutral with regard to jurisdictional claims in published maps and institutional affiliations.

ACCEPTED PAPER

Abstract

Digital light processing (DLP) bioprinting enables the fabrication of stem cell-derived liver organoids into biomimetic architectures. However, preserving quiescent hepatic stellate cells (HSCs) within human liver organoids during DLP printing remains challenging, as the mechanical requirements for print fidelity often conflict with the compliant microenvironment necessary for maintaining HSC quiescence. To address this limitation, we delineated the printable window of iPSC-derived HSCs that balances printability with resistance to activation. Notably, day 10 HSCs retained a quiescent phenotype, contributing to the assembly of multicellular organoids without fibrotic activation. We subsequently evaluated the stress relaxation properties of PEGDA-GelMA and F127DA-GelMA hydrogels, demonstrating that fast-relaxing inner hydrogels preserved compact cellular morphology of liver organoids, suppressed activation-associated gene expression, and protected HSCs from fibrotic conversion. This highlights that stress relaxation, rather than stiffness alone, is critical for cellular adaptation. Then, we developed a DLP-bioprinted macroencapsulation platform integrating stage-selected iPSC-derived HSCs, stress relaxation-tuned hydrogels, and a protective outer shell. The DLP-printed outer shell conferred structural integrity to the macroencapsulated construct, enabling successful implantation in immunocompetent mice with high graft viability and minimal αSMA expression in iPSC-derived liver organoids containing HSCs. In summary, this study establishes a coordinated strategy harmonizing HSC selection, matrix mechanics, and bioprinting design to balance biological and mechanical demands, yielding structurally stable, physiologically relevant liver organoids while preventing fibrotic activation during biofabrication.

Keywords: Human liver organoids; Hepatic stellate cells; DLP bioprinting; Stress relaxation; Macroencapsulation

ACCEPTED PAPER

1. Introduction

Human liver organoids have emerged as promising in vitro models for studying liver development, disease, and regeneration since they can partially recapitulate hepatic architecture, multicellular composition, and tissue function [1-4]. Within the cellular components of liver organoids, hepatic stellate cells (HSCs) are a critical liver non-parenchymal cells that contributes to hepatic homeostasis and also regulates liver zonation, size, and tissue function [5]. In their quiescent state, HSCs store vitamin A and maintain a normal hepatic microenvironment, whereas upon activation they lose these features, acquire a myofibroblast-like phenotype, and promote extracellular matrix deposition and fibrogenesis [6]. This transition shifts the liver organoids away from a physiological baseline toward a fibrosis-like state. Accordingly, preservation of a quiescent or low-activation HSC state is important for human liver organoids that faithfully represent normal liver physiology rather than a pre-fibrotic condition. However, primary human HSCs are scarce and readily undergo spontaneous activation during isolation and in vitro expansion, thereby limiting their utility in standardized tissue models [7]. Human induced pluripotent stem cell (iPSC)-derived HSCs provide a renewable and controllable alternative and have been used for fibrosis modeling and drug screening [8].

Three-dimensional bioprinting offers liver organoids a defined mechanical microenvironment and controlled geometric architecture, enabling the recapitulation of native hepatic tissue structure [9, 10]. In particular, digital light processing (DLP)-based bioprinting exhibits practical advantages, including rapid fabrication, high structural fidelity, and relatively low shear stress during processing [9, 11, 12], rendering it particularly suitable for replicating the hierarchical architecture of native organs while providing mechanical protection for sensitive cell populations during transplantation [13, 14]. However, current DLP hydrogel formulations often prioritize matrix stiffness to ensure printing fidelity and fabrication efficiency [15], potentially compromising HSCs quiescence maintenance within liver organoids, given the pronounced mechanosensitivity of these cells and their propensity for activation upon matrix stiffening [6]. Therefore, the fabrication of structurally and functionally biomimetic liver organoids via DLP bioprinting necessitates consideration of the mechanical compatibility between the printed hydrogel matrices and the mechanosensitivity of HSCs.

ACCEPTED PAPER

Here, we established a DLP-printable human liver organoid platform that preserved HSC quiescence and enabled transplantation in immunocompetent mice. We achieved the maintenance of quiescence in printed liver organoids through the optimization of both the printable window for iPSC-derived HSCs and the mechanical properties of DLP-printed hydrogel matrices. Subsequently, we employed DLP bioprinting to fabricate a macroencapsulated construct comprising an organoid-compatible inner matrix encased within a DLP-bioprinted outer shell, yielding stable and viable grafts devoid of fibrotic activation. This study establishes a biofabrication framework for liver organoid generation and transplantation that preserves the quiescent phenotype of HSCs.

2. Materials and methods

2.1 Differentiation of iPSC to hepatic stellate cells, endothelial cells and hepatoblast

Human induced pluripotent stem cells (hiPSCs, Nuwacell, RC01001-A) were cultured with ncTarget medium (Nuwacell, RP01020). When the cells reached approximately 80% confluence, subculture was carried out at a ratio of 1:10.

For HSCs differentiation, iPSCs were sequentially induced through mesodermal, mesenchymal/mesothelial, and HSC specification stages, as outlined in Fig. 1A, following an adapted protocol based on Coll et al. Mesoderm induction was performed from day 0 to day 4 in basal medium supplemented with BMP4 (PeproTech, 96-120-05), followed by mesenchymal/mesothelial patterning from day 4 to day 8 using BMP4, FGF1 (PeproTech, 100-17A), and FGF3 (BioLegend, 558004), with retinol (Sigma-Aldrich, R7632-100MG), palmitic acid (Sigma-Aldrich, P0500), and B27 minus insulin (Gibco, A1895601) added from day 6. Cells were subsequently matured toward an HSC-like fate from day 8 to day 12 in MCDB-201 basal medium (Sigma-Aldrich, M6770) containing retinol, palmitic acid, and B27 minus insulin.

For endothelial differentiation, hiPSCs were seeded onto Matrigel-coated plates, cultured with ncTarget medium supplemented with 1 μM CHIR99021 (Selleck, S1263) and cultured overnight. From day 0-1, the medium was RPMI1640 (Thermofisher, 11875119) supplemented with B27 insulin minus (Gibco, A1895601), 50 ng/mL Activin A (R&D, 338-AC) and 1/60 Matrigel (BD, Growth Factor Reduced, 354230). From days 1-2, the medium was changed to RPMI 1640 supplemented with B27 insulin minus, 40 ng/mL BMP4 (PeproTech, 96-120) and 1 μM

ACCEPTED PAPER

CHIR99021. From days 2-5, the medium was changed to Vivo15 (Lonza, BE02-060F) supplemented with ITS (Merck, I3146), 500 μM monothioglycerol (Sigma-Aldrich, M6145), GlutaMax (Gibco, 35050061), 50 μg/mL ascorbic acid (Sigma-Aldrich, A8960), 0.1% BSA (Sigma-Aldrich, V900933), 300 ng/mL VEGF (R&D Systems, 293-VE), 5 ng/mL FGF2 (PeproTech, 96-100-18B) and 10 ng/mL BMP4 (PeproTech, 96-120). On day 5, we obtained endothelial progenitor cells to generate liver organoids (LOs).

For hiPSC differentiation towards the hepatic lineage, hiPSCs were seeded onto Matrigel-coated plates with ncTarget medium and cultured overnight. From day 0-1, the medium was RPMI1640 supplemented with B27 insulin minus and 3 μM CHIR99021. From days 2-3, the medium was changed to RPMI 1640 supplemented with B27 insulin minus and 100 ng/mL Activin A. From days 5-8, the medium was changed to RPMI 1640 supplemented with B27 (Gibco, A1486701), 20 ng/mL BMP4, and 10 ng/mL FGF2 for hepatoblast induction. On day 8, we obtained hepatoblast cells to generate LOs.

2.2 The assessment of iPSC-derived HSC activation

To assess activation competence, day 12 iPSC-derived HSCs were exposed to recombinant TGFβ (R&D Systems, 240-B) at 10 ng/ml for 24 h. Activation was determined by immunostaining for αSMA and analysis of fibrosis-associated gene expression. Morphological changes during extended culture were documented by fluorescence imaging through day 14.

Spontaneous autofluorescence of day 12 HSCs was examined as a functional feature associated with HSC maturation. Fluorescence was imaged using a laser scanning at 340 nm confocal microscope system (LSCM, Nikon) under filter settings, and changes during continued culture were compared qualitatively with the emergence of a fibrotic phenotype.

2.3 Assembly of multicellular liver organoids with iPSC-derived HSCs

To determine the optimal differentiation stage of iPSC-derived HSCs for organoid assembly, HSCs harvested on day 10 or day 12 were combined with endothelial cells and hepatocyte-lineage cells to generate multicellular aggregates in AggreWell plates (Stemcell, 34415). Single-cell suspensions were prepared via dissociation with Accutase (STEMCELL Technologies, 07920). The three cell populations were subsequently combined at a stoichiometric ratio of 1:1:1 (HSCs: ECs: hepatoblasts) to ensure uniform multicellular integration.

ACCEPTED PAPER

Cells were seeded into microwells and maintained in a specialized organoid culture medium. This basal medium consisted of a 1:1:1 mixture of DMEM/F-12 (Gibco, 11320033), Medium 199 (Gibco,11150059), and William's E Medium (Gibco, 12551032), supplemented with 500 μM monothioglycerol, B27, 1% ITS, 50 μg/mL ascorbic acid, 0.1% BSA, 2% FBS, 1% sodium pyruvate (Sigma, P2256), 1% MEM NEAA, 1% GlutaMAX, 20 ng/mL VEGF, 20 ng/mL HGF (PeproTech, 96-100-39), 20 ng/mL Oncostatin M (PeproTech, 96-300-10), and 5 ng/mL FGF2. The medium was refreshed every other day.

2.4 Hydrogel preparation and rheological characterization

To investigate the role of matrix viscoelasticity in regulating liver organoid behavior, two DLP-printable hydrogel systems were prepared with comparable stiffness but distinct stress-relaxation properties: 1% PEG10000DA (Sigma-Aldrich,455008)–5% GelMA (EFL, EFL-GM-60) and 1% F127DA (EFL, EFL-F127DA)–5% GelMA. PEG10000DA, F127DA and GelMA were dissolved in DPBS containing LAP (Sigma-Aldrich,900889) at 16 mM, 0.8 mM Tartrazine (Sigma-Aldrich, T0388).

Mechanical properties were measured using a rheometer (Anton Paar, MCR302e). Briefly, the rheometer was equipped with a cone plate with 25 mm diameter, 99 μm truncation gap, and 2° cone angle. The platform temperature was set at 37 ℃. The storage modulus (G′) was determined under oscillatory shear at 1 Hz. Stress-relaxation testing was performed by applying a constant strain of 5% and recording stress decay over time. The linear limit of the strain was analyzed by Analysis Window in RheoPlus software with a smoothing range of 5% to obtain the G′ and G″ values under different conditions. Hydrogels with matched G′ but distinct relaxation profiles were selected for subsequent studies. Under these conditions, PEGDA–GelMA behaved as a slow-relaxing matrix, whereas F127DA–GelMA exhibited rapid stress relaxation.

2.5 Encapsulation of liver organoids in hydrogels

Preformed liver organoids were resuspended in hydrogel precursor solutions and encapsulated by photocrosslinking using a DLP-based printing or light-curing system (Cellink, Lumen x+). Crosslinking was performed for 4 s and 30 mW/cm^2 of 405 nm under sterile conditions. Organoid-laden constructs were maintained in organoid culture medium for 2 days. The transplanted liver organoids have a size of approximately 100 μm, with a number of around 100 organoids per mouse.

ACCEPTED PAPER

Organoid morphology within the hydrogels were evaluated by brightfield and fluorescence microscopy. Morphological parameters, including organoid compaction, outward migration and interaction with the surrounding matrix, were assessed qualitatively using Nikon NIS-Elements AR. To determine the effect of matrix relaxation on HSC-associated transcriptional programs, RNA was isolated from encapsulated organoids after 2 days of culture and analyzed by qRT–PCR for PDGFRB, HGF, GFAP, LOXL2, ACTA2 and TIMP1.

2.6 DLP bioprinting of macroencapsulated liver organoid constructs

For macroencapsulation, a core–shell construct was designed using 14% F127DA–5% GelMA as the outer protective layer and 1% F127DA–5% GelMA as the inner cell-laden compartment containing liver organoids. Printing was performed using a DLP bioprinter under sterile conditions. Printing parameters, including the layer thickness of 100 μm, exposure time of 4 s per layer at light intensity of 20 mW/cm², cumulative light dose of 80 mJ/cm² per layer, were optimized to balance structural fidelity and cell survival. Construct integrity was assessed immediately after printing by gross inspection and microscopy.

2.7 Subcutaneous implantation and histological analysis

All animal experiments were approved by the Institutional Animal Care and Use [MDL2024-09-27-01] and performed in accordance with relevant institutional guidelines. Immunocompetent mice (C57BL, male, 4 weeks) were used for subcutaneous implantation studies.

To evaluate in vivo material stability, acellular hydrogels with identical morphology composed of 8% F127DA–5% GelMA or 14% F127DA–5% GelMA were implanted subcutaneously. At 14 days post-implantation, implants were retrieved and assessed for gross retention and degradation. Explanted tissues and major organs of the mice were fixed in 4% paraformaldehyde (PFA; Sigma-Aldrich, 158127), embedded in paraffin (Sigma-Aldrich, P3558), sectioned, and stained with H&E and Masson’s trichrome (Sigma-Aldrich, HT15) to evaluate host response, collagen deposition and fibrotic encapsulation.

For transplantation studies, bioprinted organoid-containing core–shell constructs were implanted subcutaneously using the same procedure. At the indicated endpoint, constructs were harvested for histology, viability assessment and immunostaining. Fibrotic activation within explanted constructs was evaluated by staining for αSMA (Abcam, ab5694).

ACCEPTED PAPER

2.8 Fluorescent live/dead staining

Fluorescent live/dead staining was used to evaluate cell viability. Briefly, specimens were incubated with 1 μM Calcein-AM (Sigma-Aldrich, 17783) and 2 μM propidium iodide (Sigma-Aldrich, P4170) for 15 min to stain live (green) and dead cells (red) in the dark. A laser scanning confocal microscope system (LSCM, Nikon, C2) was used to acquire the images. The count/size tool Image-Pro-Plus 6.0 was used to quantify the live and dead cells.

2.9 Immunofluorescence staining

Samples were fixed with 2.5% glutaraldehyde (Sigma Aldrich, G5882), permeabilized with 0.1% Triton-X 100 (Sigma, T8787), blocked with 10% BSA, and then incubated with primary antibody (ALCAM, PDGFRB, αSMA, NCAM, RELN, COL1A1) at 4 °C overnight, followed by incubation with the corresponding secondary antibody. The negative controls were obtained by replacing the primary antibodies with corresponding immunoglobulin G antibodies. DAPI (Sigma, D9542) or Hoechst (Invitrogen, H3570) was used to visualize the cell nuclei. LSCM was used to obtain the images.

2.10 qRT-PCR assay

qRT-PCR was performed to determine the expression levels of different genes. Briefly, cells were harvested from the liver models, and total RNA was extracted with TRIzol (Invitrogen). A cDNA synthesis kit (Takara, 6210) was used for reverse transcription according to the manufacturer's instructions, and qRT-PCR was performed on a real-time PCR detection platform (Bio-Rad, CFX96) with Maxima SYBR Green qPCR master mix (Thermo Scientific). Each sample was analyzed in triplicate. The housekeeping gene glyceraldehyde3-phophate dehydrogenase (GAPDH) was used as an internal control for normalization.

2.11 Statistical analysis

Data are presented as mean ± s.d, as indicated in the figure legends. All experiments were performed with at least three independent biological replicates. Statistical analyses were performed using GraphPad Prism 9.5. Two-group comparisons were performed using two-tailed unpaired Student’s t-tests. Multiple-group comparisons were analyzed using one-way ANOVA. Differences were considered statistically significant as shown in the figure legends.

ACCEPTED PAPER

3. Results

3.1. Differentiation and Activation of iPSC-Derived HSCs

We first differentiated iPSCs into HSCs (Figure 1A). During the differentiation process, we observed a significant upregulation of *KDR* transcriptional expression during the mesodermal stage (D0-D4), followed by increased expression of *P75NTR*, *ALCAM*, *VIM*, and *PCDH7* during the mesenchymal and mesothelial cell stages (D4-D8) (Figure 1B, C). Furthermore, negative expression of SSEA4 and positive expression of ALCAM indicated successful differentiation into hepatic stellate progenitor cells (Figure 1C). By D12, the transcriptional expression of *NCAM*, *PDGFRB*, *RELN*, *HGF*, *COL1A1*, *ACTA2*, and *PPARG* was significantly upregulated (Figure 1B), along with positive expression of HSC identity marker PDGFRB and ALCAM (Figure 1C). We found that most cells at day 12 remained quiescent with a subtle expression of αSMA, compared with fibroblast cells (Figure 1C). Additionally, Day 12 cells can be activated by TGFβ, showing increased αSMA expression (Figure 1D, E, Figure S1), indicating their responsiveness to fibrotic stimuli. However, prominent fibrosis was observed at Day 14 with increasing expression of αSMA, suggesting that HSCs could not maintain a quiescent state for extended periods under the current culture conditions (Figures 1D, E). Furthermore, spontaneous fluorescence of HSCs in Day 12, a hallmark of functional maturity, diminished with extended culture (Figure 1F), indicating that iPSC-derived HSCs underwent fibrosis in culture, which complicated their use for applications requiring quiescent HSCs (Figure 1G).

ACCEPTED PAPER

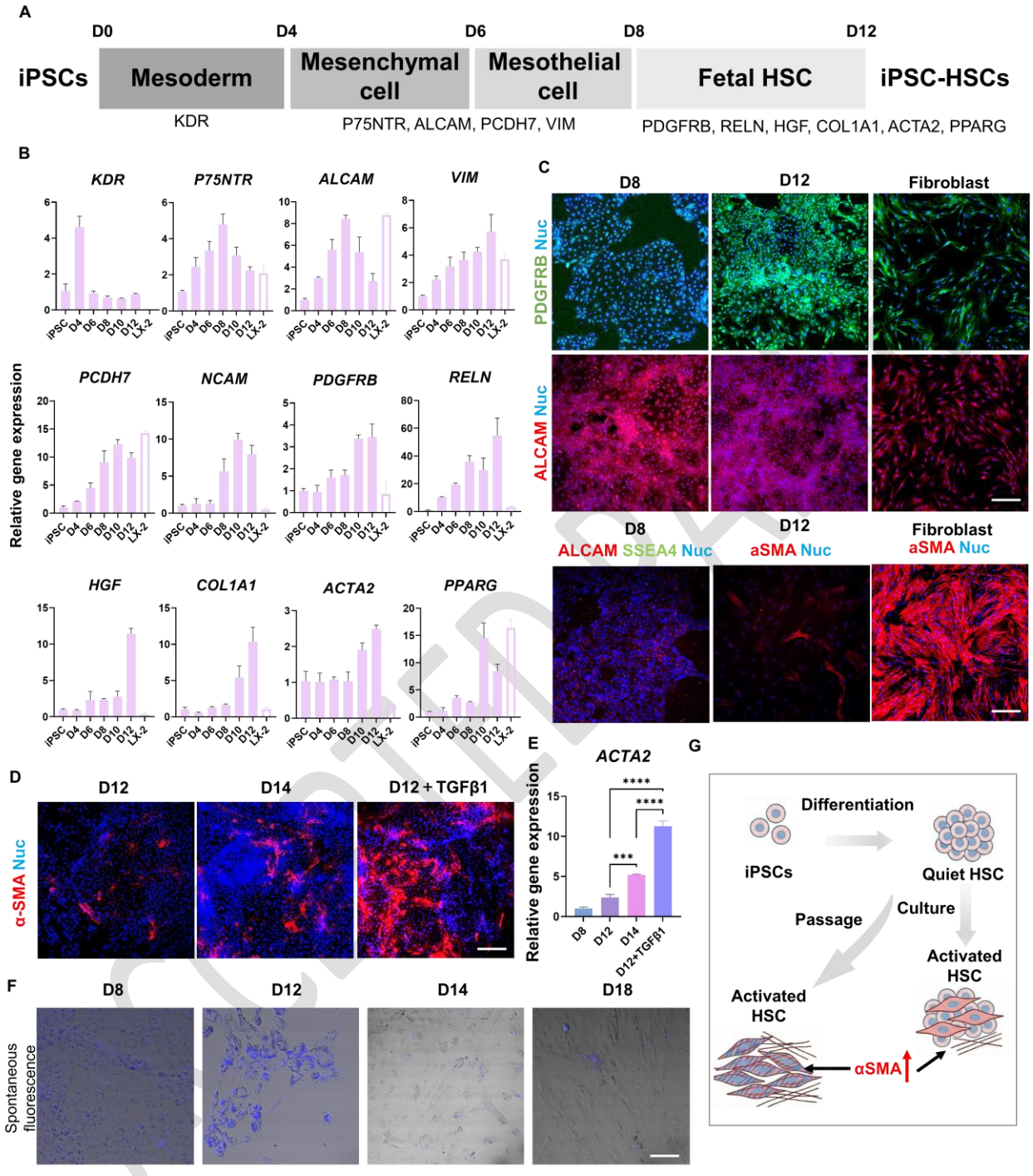


Figure 1. Stepwise differentiation and activation profiling of iPSC-HSCs. (A) Schematic of the differentiation trajectory from iPSCs to iPSC-HSCs. (B) Temporal expression of indicated lineage markers during differentiation. (C and D) Representative immunofluorescence images showing marker expression at indicated stages and after TGFβ1 treatment. Three experimental groups are defined as follows: D12 represents day 12 of differentiation; D14 represents day 14 of

differentiation; D12+TGFβ represents the cells at day 12 with TGFβ1 treatment for additional two days. (E) Quantification of ACTA2 expression. (F) Representative spontaneous fluorescence images during culture. Scale bar=200 μm. (G) Schematic of iPSC-HSC differentiation, culture-dependent activation, and αSMA upregulation. Data are mean ± SD; ns, not significant; ***$p < 0.001$, ****$p < 0.0001$.

3.2. iPSC-Derived Immature HSCs are Suitable for Organoid Formation with a Quiescent Phenotype

After differentiating iPSCs into HSCs for 10 or 12 days, we separately co-cultured the HSCs with iPSC derived endothelial cells and hepatocytes in Aggrewell plates (Figure 2A). These two types of iPSC-derived HSCs contribute to the formation of compact cell aggregates, indicating the mesenchymal feature (Figure 2B). Immunostaining showed that the LOs containing iPSC-derived HSCs at day 10 (LOs_D10) positively expressed the biomarker PDGFRB with minimal expression of αSMA, indicating a more quiescent state. In contrast, LOs containing iPSC-derived HSCs at day 12 (LOs_D12) exhibited increased expression of αSMA, indicating the activated state of HSCs (Figure 2B, Figure S2). Gene expression demonstrated that LOs_D10 displayed lower expression of fibrosis-related genes, including *ACTA2* and *TIMP1*, compared to that of LOs_D12 (Figure 2C). These results suggests that Day 10 HSCs are more suited for generation of physiological liver organoids maintaining a more quiescent phenotype.

ACCEPTED PAPER

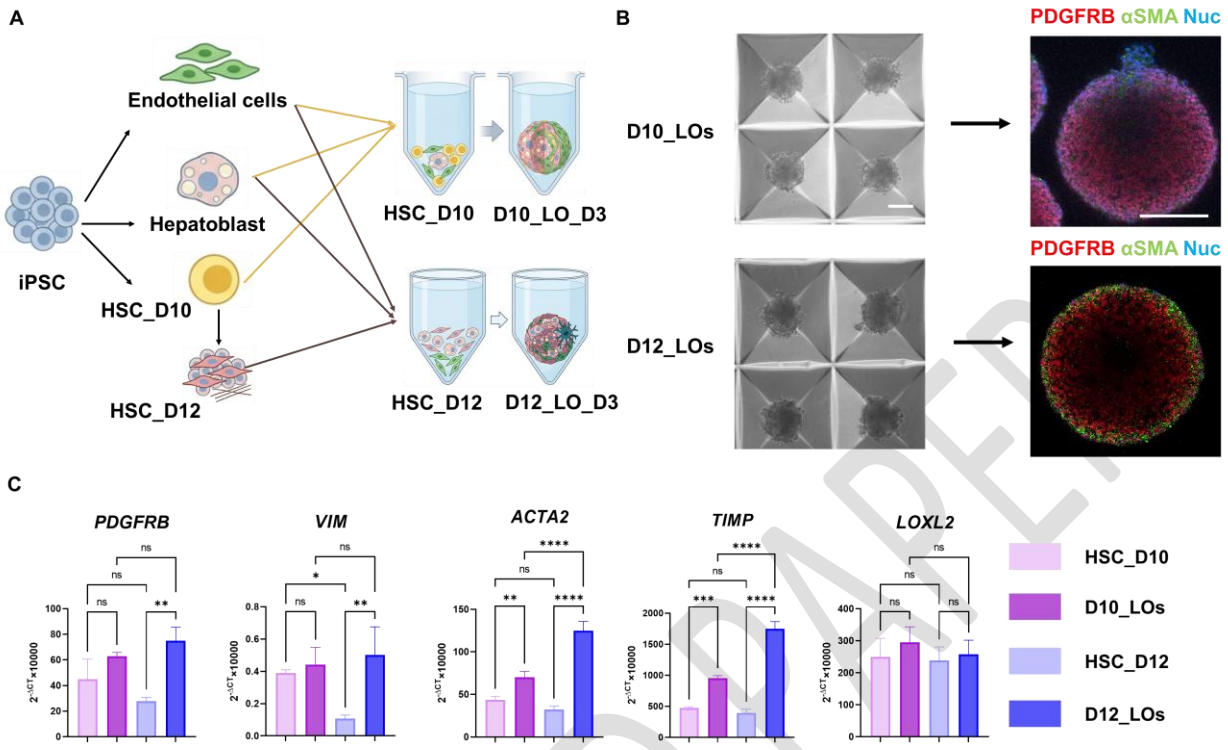


Figure 2. iPSC-derived HSCs at day 10 are suitable for organoid formation with a quiescent phenotype. (A) Schematic of iPSC differentiation into HSCs and co-culture with endothelial and hepatocyte cells in 3D conditions. (B) Morphology of Day 10 and Day 12 HSCs cultured in 3D matrices (D10_LOs and D12_LOs), scale bars, 50 μm. Immunofluorescence images showing PDGFRB (red) and αSMA (green), scale bars, 50 μm. (C) Gene expression analysis of HSC markers. Data are mean ± SD; ns, not significant; ***p < 0.001, ****p < 0.0001.

3.3. Matrix Stress Relaxation Regulates Liver Organoid Morphology and HSC-Associated Gene Expression

To explore the effect of the matrix viscoelasticity on the active state of LOs_D10, we established two kinds of DLP-printable hydrogel systems with comparable stiffness but distinct stress-relaxation properties: 1% PEGDA-5% GelMA and 1% F127DA-5% GelMA (Figures 3A). Both hydrogels exhibited comparable storage modulus (G′) around 500 Pa within the physiological range of the liver ECM (Figures 3B). PEGDA-GelMA retained higher residual stress and behaved as a slow-relaxing matrix, whereas F127DA-GelMA exhibited a fast-relaxing profile (Figures 3C, 3D). When LOs_D10 was encapsulated in these matrices, we observed obvious differences in the

ACCEPTED PAPER

morphology: LOs_D10 in slow-relaxing PEGDA-GelMA exhibited more pronounced outward migration (Figures 3E) and stronger interactions with the surrounding matrix (Figures 3F), while those in fast-relaxing F127DA-GelMA retained a compact spherical structure with reduced migration (Figures 3E) and weaker interfacial attachment (Figures 3F). By analysis the gene expression of LOs_D10, fast-relaxing matrix upregulated the genes related to functional mature, like *PDGFRB*, *HGF*, and *GFAP*, whereas slow-relaxing matrix preferentially increased expression of genes associated HSC activation, such as *LOXL2*, *ACTA2*, and *TIMP1* (Figure 3G). These findings indicate that at modulus within the physiological range of the liver, fast-relaxing matrices promote a more quiescent phenotype, whereas slow-relaxing matrices mimic fibrotic environments that drive HSC activation.

ACCEPTED PAPER

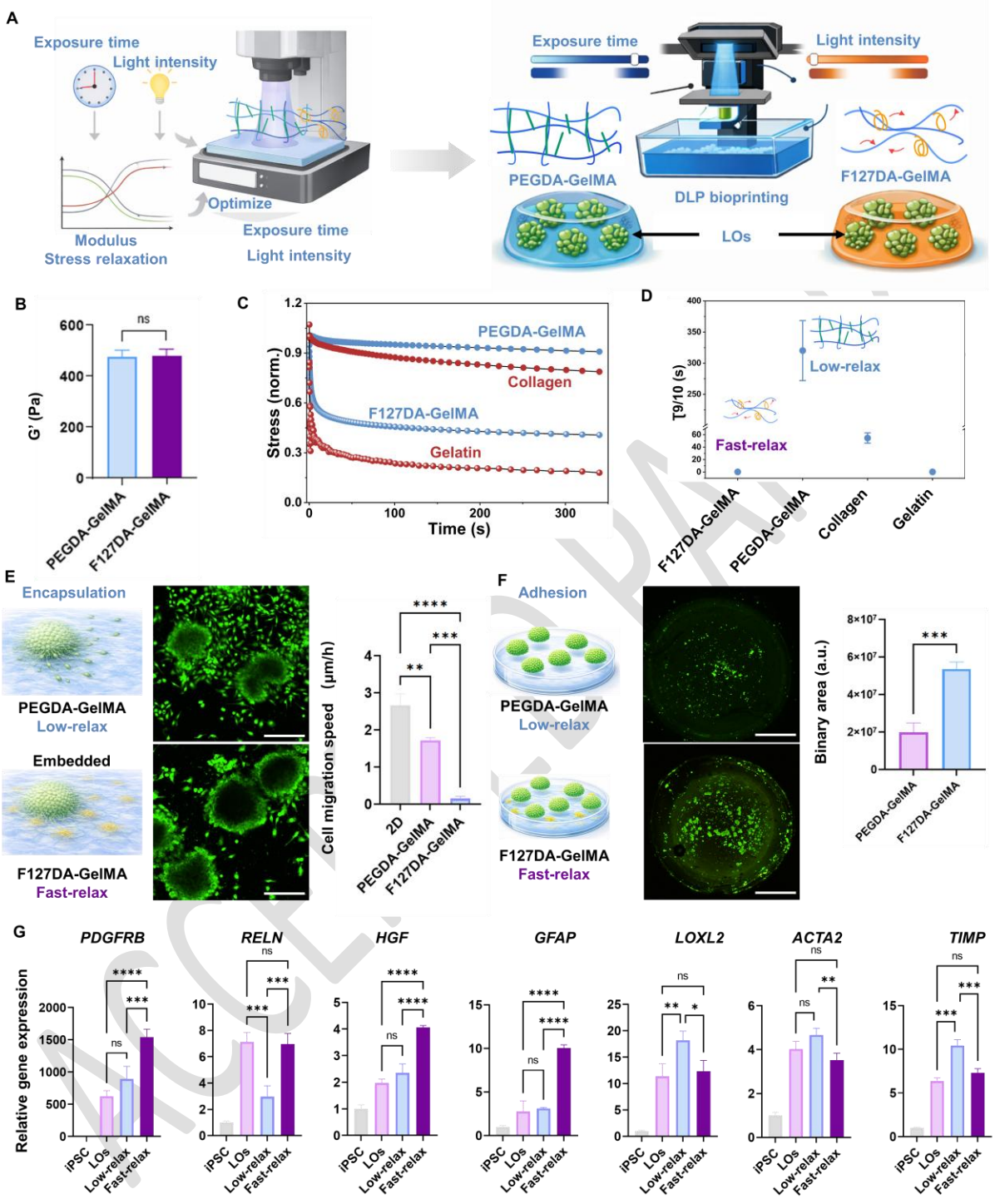


Figure 3. Hydrogel viscoelasticity regulates LOs behavior. (A) Schematic of photorheology-guided hydrogel optimization and DLP bioprinting. (B) Storage modulus (G′) of hydrogels. (C and D) Stress-relaxation curves and quantification. (E and F) Representative images and quantification

of cell migration. Scale bar, 200 μm. (G) Relative expression of genes. Data are mean ± SD; ns, not significant; *p < 0.05, **p < 0.01, ***p < 0.001, ****p < 0.0001.

3.4 DLP Bioprinted Hydrogel Construct Encapsulating Liver Organoid

To 3D print macroencapsulated hydrogels for in vivo transplantation of liver organoids, we first examined the structural integrity of F127DA-GelMA hydrogels at different concentrations following subcutaneous implantation in immunocompetent mice. By day 14, 8% F127DA-GelMA had undergone substantial degradation, leaving minimal residual material, whereas 14% F127DA-GelMA maintained its structure without significant degradation or signs of inflammation (Figures 4A). Histological analysis confirmed greater hydrogel retention in the 14% F127DA-GelMA group, with no notable collagen deposition or fibrotic encapsulation around the implant (Figure 4B, Figure S3). This long-term stability and low fibrosis are critical for supporting cell transplantation in immunocompetent mice. We did not observe any obvious pathological changes in the organs of mice 14 days after transplantation with 14% F127DA-GelMA (Figure S4). Based on these results, we designed a composite bioprinted construct consisting of a 14% F127DA–5% GelMA outer protective shell and a 1% F127DA–5% GelMA ECM-mimicking inner compartment to encapsulate Day 10 liver organoids (Figure 4C). The printed constructs exhibited robust structural integrity and high cell viability (Figures 4D). Following subcutaneous implantation, the constructs remained intact and localized at the implantation site for at least 14 days (Figures 4E), maintaining cell viability (Figures 4F) and showing no significant increase in αSMA expression, indicating the maintenance of LOs_D10 in a quiescent phenotype (Figure 4G). These results support the use of the F127DA-GelMA DLP bioprinting platform as a biocompatible macroencapsulation strategy for in vivo delivery of iPSC-derived liver organoids in immunocompetent hosts.

ACCEPTED PAPER

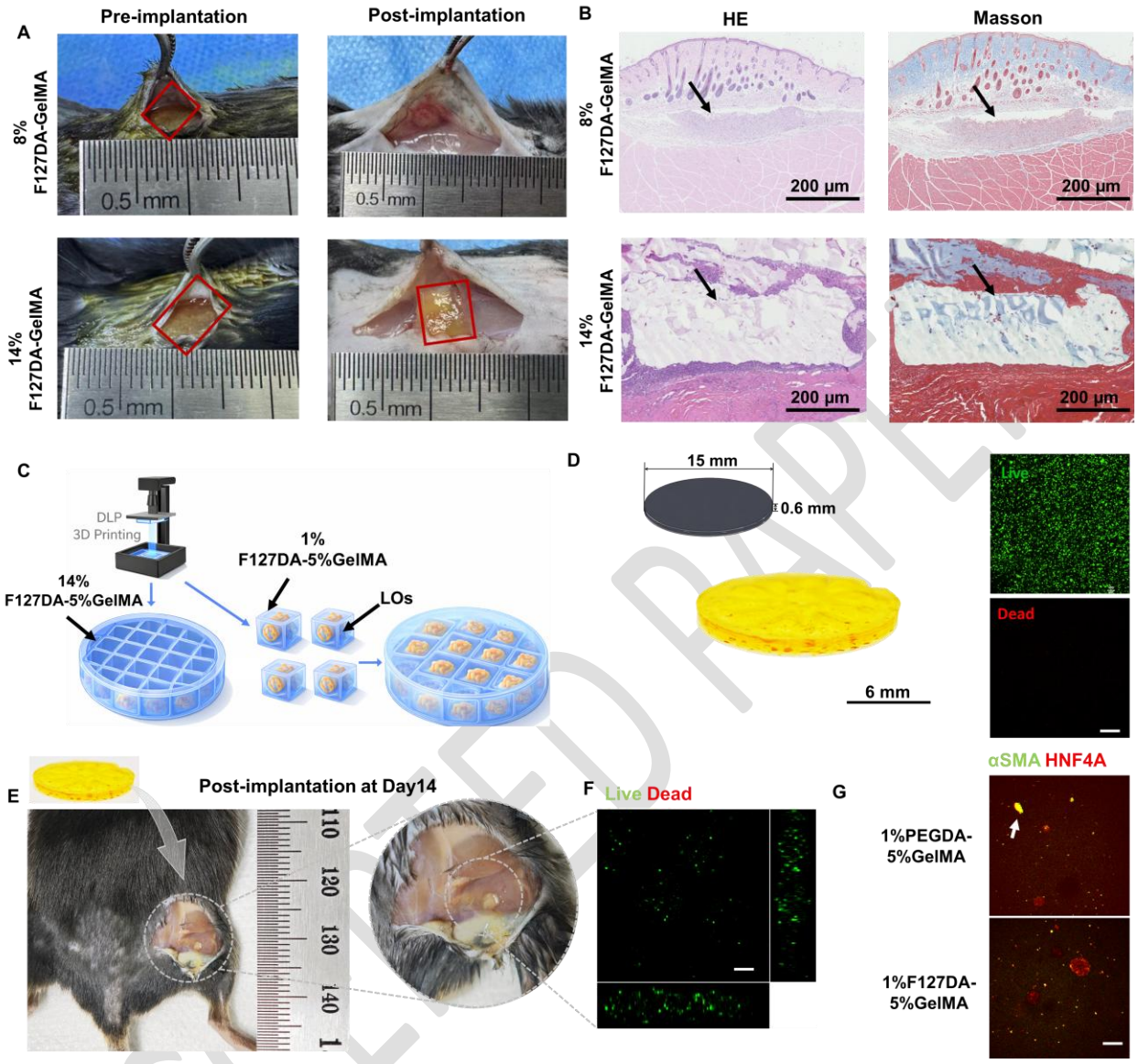


Figure 4. In vivo validation of bioprinted hydrogels and liver organoids. (A and B) Gross images and histology of implanted hydrogels at indicated compositions. (C) Schematic of DLP bioprinting and encapsulation of LOs_D10. Representative images of printed constructs (D, E) and live/dead staining after printing (D) and implantation (F). Scale bar, 200 μm. (G) Representative histological analysis of implanted constructs.

ACCEPTED ARTICLE

4. Discussion

We established a DLP-printable liver organoid platform that addresses the challenge of maintaining HSC quiescence in mechanically sensitive constructs. By integrating stage-selected iPSC-derived HSCs, a fast stress-relaxing hydrogel, and macroencapsulation, we generated spatially defined, transplantable organoids that preserve HSC low-activation states while enabling high-fidelity printing and structural stability. This approach overcomes the mechanical stresses inherent to DLP bioprinting and provides a practical strategy for building organoid constructs suitable for in vivo transplantation.

HSCs are increasingly recognized as regulators of liver zonation, regeneration, metabolism, and organoid maturation, rather than merely fibrogenic effector cells [5]. Pluripotent stem cells can be differentiated into quiescent HSC-like cells, providing a practical human cell source that helps overcome the limited availability of primary cells [7]. Our results support the reproducibility of this differentiation strategy across laboratories, but also highlight an important limitation. Although day 12 iPSC-derived HSCs displayed features associated with HSC maturation, this state was transient and readily shifted toward activation with continued culture. Compared with day 12 cells, day 10 iPSC-derived HSCs retained HSC identity, supported multicellular organoid assembly, and showed lower expression of fibrosis-associated genes. These findings suggest that the most suitable HSC population for building physiological liver organoids is not necessarily the most mature one, but the one least prone to activation during subsequent culture.

To better preserve organoid quiescence after DLP printing, we sought to define the relevant hydrogel mechanical features. PEGDA-GelMA and F127DA-GelMA were selected to provide comparable initial stiffness but distinct stress-relaxation profiles. Both PEGDA and F127DA are widely used synthetic polymers that are relatively bioinert and lack intrinsic cell-adhesive motifs [16, 17], whereas GelMA provides cell-interactive sites such as RGD sequences. Since both formulations contained the same GelMA concentration, the major bioactive ligand component was kept comparable between groups, while PEGDA and F127DA mainly served as tunable network-forming components. By comparing hydrogels with matched stiffness but distinct stress-relaxation profiles, we identified stress relaxation as an independent regulator of liver organoid state. Slow-relaxing PEGDA-GelMA promoted outward migration and higher expression of activation-associated genes, whereas fast-relaxing F127DA-GelMA preserved compact morphology and

ACCEPTED PAPER

favored quiescence-associated markers. Previous work reported that relaxation of matrix mechanics can partially, although incompletely, reverse HSC activation [18]. These results suggest that matrix stress relaxation is closely associated with HSC phenotype regulation, beyond the effect of initial stiffness alone. As recent reviews have emphasized, printing-compatible materials should support not only structural fidelity, but also functional homeostasis [9]. Our results therefore suggest that, in printable liver organoid systems, hydrogel design for HSC-containing constructs should account not only for stiffness, but also for force dissipation. Nevertheless, PEGDA-GelMA and F127DA-GelMA are not chemically identical. Future studies using chemically matched or independently tunable viscoelastic hydrogels will be needed to more precisely define the role of relaxation kinetics in HSC fate regulation.

For DLP-printed constructs intended for implantation, sufficient mechanical support is required to maintain structural integrity during handling and after implantation, which often necessitates a relatively high modulus [19]. This poses a particular challenge for liver organoids containing hepatic stellate cells that are sensitive to mechanical cues. To address this, we used DLP printing to spatially separate mechanical and biological functions by constructing a mechanically supportive outer hydrogel shell and an inner hydrogel compartment encapsulating the organoids. In our system, the fast-relaxing inner matrix preserved quiescence-associated features without an immediate increase in αSMA, while the supportive outer hydrogel shell enabled implantation in immunocompetent mice. Although we have not yet assessed long-term functional outcomes, these results suggest that an organoid state established through stress-relaxation-guided matrix selection can withstand DLP fabrication, macroencapsulation, and implantation in immunocompetent hosts without immediately drifting toward αSMA-associated fibrotic activation. Compared with previous encapsulation-based studies, our system extends this concept to multicellular liver organoids containing HSCs and emphasizes preservation of HSC quiescence [20].

The limitation of this study is that longer-term in vivo investigations are required to determine whether these constructs can stably maintain long-term graft stability, hepatocyte-specific functions, vascularization, immune infiltration, fibrotic capsule maturation, and sustained maintenance of the liver organoid phenotype. Nevertheless, our work establishes a feasible framework for generating bioprinted and transplantable human liver organoids. This framework

ACCEPTED PAPER

emphasizes the maintenance of a low-activated HSC baseline throughout cell selection, matrix design, and subsequent implantation.

5. Conclusion

We developed a DLP-bioprinted macroencapsulation system for human liver organoids that maintained stellate cells in a low-activation state. Day 10 iPSC-derived HSCs were more suitable for organoid assembly than day 12 cells, and fast stress-relaxing hydrogels better preserved organoid morphology and quiescence-related features than stiffness-matched slow-relaxing matrices. The core-shell construct supported high viability and remained stable after implantation in immunocompetent mice, providing a practical basis for building transplantable liver organoids and future functional evaluation studies.

Funding
This work was supported by the National Natural Science Foundation of China (22534006), and the Tianjin Natural Science Foundation Project (23JCQNJC00790).

Conflict of interest
The authors declare that they have no known competing financial interests or personal relationships that could have appeared to influence the work reported in this paper.

Author contributions
Conceptualization: Zhi Zhou, Xiaodong Ding
Formal analysis: Ruitong Li, Xiaodong Ding
Investigation: Zhi Zhou, Ruitong Li, Xiaodong Ding
Methodology: Ruitong Li, Xiaodong Ding, Yixuan Li
Writing–original draft: Shaojun Liang
Writing–review & editing: Ruitong Li, Yixue Luo

Ethics approval and consent to participate
All animal experiments were approved by the Institutional Animal Care and Use [MDL2024-09-27-01] and performed in accordance with relevant institutional guidelines.

Consent for publication
Not applicable.

ACCEPTED PAPER

References

1. Takebe, T.; Sekine, K.; Enomura, M.; Koike, H.; Kimura, M.; Ogaeri, T.; Zhang, R.-R.; Ueno, Y.; Zheng, Y.-W.; Koike, N.; Aoyama, S.; Adachi, Y.; Taniguchi, H., Vascularized and functional human liver from an iPSC-derived organ bud transplant. Nature 2013, 499 (7459):481-484. doi: 10.1038/nature12271

2. Tang, X.-Y.; Wu, S.; Wang, D.; Chu, C.; Hong, Y.; Tao, M.; Hu, H.; Xu, M.; Guo, X.; Liu, Y., Human organoids in basic research and clinical applications. Signal Transduction and Targeted Therapy 2022, 7(1):168. doi: 10.1038/s41392-022-01024-9

3. Harrison, S. P.; Baumgarten, S. F.; Verma, R.; Lunov, O.; Dejneka, A.; Sullivan, G. J., Liver Organoids: Recent Developments, Limitations and Potential. Front Med (Lausanne) 2021, 8:574047. doi: 10.3389/fmed.2021.574047

4. Grebenyuk, S.; Abdel Fattah, A. R.; Kumar, M.; Toprakhisar, B.; Rustandi, G.; Vananroye, A.; Salmon, I.; Verfaillie, C.; Grillo, M.; Ranga, A., Large-scale perfused tissues via synthetic 3D soft microfluidics. Nat Commun 2023, 14 (1):193. doi: 10.1038/s41467-022-35619-1

5. Kamm, D. R.; McCommis, K. S., Hepatic stellate cells in physiology and pathology. J Physiol-London 2022, 600 (8):1825-1837. doi: 10.1113/JP281061

6. Trivedi, P.; Wang, S.; Friedman, S. L., The Power of Plasticity—Metabolic Regulation of Hepatic Stellate Cells. Cell Metab 2021, 33 (2):242-257. doi: 10.1016/j.cmet.2020.10.026

7. Coll, M.; Perea, L.; Boon, R.; Leite, S. B.; Vallverdu, J.; Mannaerts, I.; Smout, A.; El Taghdouini, A.; Blaya, D.; Rodrigo-Torres, D.; Graupera, I.; Aguilar-Bravo, B.; Chesne, C.; Najimi, M.; Sokal, E.; Lozano, J. J.; van Grunsven, L. A.; Verfaillie, C. M.; Sancho-Bru, P., Generation of Hepatic Stellate Cells from Human Pluripotent Stem Cells Enables Modeling of Liver Fibrosis. Cell Stem Cell 2018, 23(1):101–113. doi: 10.1016/j.stem.2018.05.027

8. Koui, Y.; Himeno, M.; Mori, Y.; Nakano, Y.; Saijou, E.; Tanimizu, N.; Kamiya, Y.; Anzai, H.; Maeda, N.; Wang, L. Y.; Yamada, T.; Sakai, Y.; Nakato, R.; Miyajima, A.; Kido, T., Development of human iPSC-derived quiescent hepatic stellate cell-like cells for drug discovery and disease modeling. Stem Cell Rep 2021, 16 (12):3050-3063. doi: 10.1016/j.stemcr.2021.11.002

ACCEPTED PAPER

9. Huang, M. S.; Christakopoulos, F.; Roth, J. G.; Heilshorn, S. C., Organoid bioprinting: from cells to functional tissues. Nat Rev Bioeng 2025, 3 (2):126-142. doi: 10.1038/s44222-024-00268-0

10. Zhao, Z. X.; Chen, X. Y.; Dowbaj, A. M.; Sljukic, A.; Bratlie, K.; Lin, L. D.; Fong, E. L.; Balachander, G. M.; Chen, Z. W.; Soragni, A.; Huch, M.; Zeng, Y. A.; Wang, Q.; Yu, H., Organoids. Nat Rev Method Prime 2022, 2(1):94. doi: 10.1038/s43586-022-00174-y

11. Ding, H. Y.; Dong, M.; Zheng, Q.; Wu, Z. L., Digital light processing 3D printing of hydrogels: a minireview. Mol Syst Des Eng 2022, 7 (9):1017-1029. doi: 10.1039/D2ME00066K

12. Jeong, Y. G.; Yoo, J. J.; Lee, S. J.; Kim, M. S., 3D digital light process bioprinting: Cutting-edge platforms for resolution of organ fabrication. Mater Today Bio 2024, 29. doi: 10.1016/j.mtbio.2024.101284

13. Duong, V. T.; Lin, C. C., Digital Light Processing 3D Bioprinting of Gelatin-Norbornene Hydrogel for Enhanced Vascularization. Macromol Biosci 2023, 23(12):e2300213. doi: 10.1002/mabi.202300213

14. Zhu S, Liao X, Xu Y, Zhou N, Pan Y, Song J, et al. 3D bioprinting of high-performance hydrogel with in-situ birth of stem cell spheroids. *Bioactive Materials*. 2025;43:392-405. doi:10.1016/j.bioactmat.2024.09.033

15. He N, Wang X, Shi L, Li J, Mo L, Chen F, et al. Photoinhibiting via simultaneous photoabsorption and free-radical reaction for high-fidelity light-based bioprinting. *Nat Commun*. 2023;14(1). doi:10.1038/s41467-023-38838-2

16. Zhu, J., Bioactive modification of poly(ethylene glycol) hydrogels for tissue engineering. *Biomaterials* 2010, 31 (17):4639-4656. doi: 10.1016/j.biomaterials.2010.02.044

17. Zhao P, Wang B, Wang L, Fu Z, Hu J, Liu Y, et al. Rapid printing of 3D porous scaffolds for breast reconstruction. *Bio-des Manuf*. 2023;6(6):691-703. doi:10.1007/s42242-023-00253-3

18. Caliari SR, Perepelyuk M, Soulas EM, Lee GY, Wells RG, Burdick JA. Gradually softening hydrogels for modeling hepatic stellate cell behavior during fibrosis regression. *Integr Biol*. 2016;8(6):720-728. doi:10.1039/c6ib00027d

ACCEPTED PAPER

19. Fowler, M.; Lozano, A. M.; Krause, J.; Bednarz, P.; Pandey, S.; Ghayour, M.; Zhang, Q. X.; Veiseh, O., Guiding vascular infiltration through architected GelMA/PEGDA hydrogels: an study of channel diameter, length, and complexity. Biomater Sci-Uk 2025, 13 (11):2951-2960. doi: 10.1039/D5BM00193E

20. Wang, Y. Q.; Huang, R. Q.; Lu, Y. G.; Liu, M. Q.; Mo, R., Immuno-protective vesicle-crosslinked hydrogel for allogenic transplantation. Nat Commun 2024, 15 (1):5176. doi: 10.1038/s41467-024-49135-x

ACCEPTED PAPER